8-5-2011

Spin and Exchange Coupling for Ti Embedded in a Surface Dipolar Network

Pushpa Raghani
Boise State University

Jesus Cruz
Georgetown University

Barbara Jones
IBM, Almaden Research Center

DOI: 10.1103/PhysRevB.84.075422

Spin and exchange coupling for Ti embedded in a surface dipolar network

Raghani Pushpa*[1,2,4], Jesus Cruz[3,2], and Barbara Jones[2]
[1] *Center for Probing the Nanoscale, Stanford University, Stanford, California, USA*
[2] *IBM, Almaden Research Center, San Jose, CA, USA*
[3] *Georgetown University, Washington, D.C., USA and*
[4] *Boise State University, Boise, Idaho, USA*

(Dated: July 12, 2011)

We have studied the spin and exchange coupling of Ti atoms deposited on a Cu2N/Cu(100) surface using density functional theory with generalized gradient approximation + U. In agreement with experiments, we find that Ti has the highest binding on top of Cu atoms. We also find that the spin of individual Ti atoms deposited on the Cu2N/Cu(100) surface increases as Ti coverage on the surface is decreased. For U=0, the spin of a Ti atom starts at S=0 at high coverages and increases to S=1/2 as the coverage is decreased, which agrees very well with results obtained from STM experiments. At higher values of U, the spin of Ti is found to be close to 1 regardless of coverage. We also calculate the exchange coupling for Ti dimers on the Cu2N/Cu(100) surface and we find that the exchange coupling across a 'void' of 3.6Å is antiferromagnetic, whereas indirect (superexchange) coupling through a N atom is ferromagnetic. For a square lattice of Ti on Cu2N/Cu(100), we find a novel spin striped phase.

PACS numbers: 71.15.Mb, 71.70.Gm, 71.15.Nc, 68.55.-a,

I. INTRODUCTION

Atomic-scale magnetic structures adsorbed on surfaces[1] are of current interest for several reasons: Primarily, they display intriguing physical properties in their own right. Magnetic nanostructures on surfaces, simple or complex, can exhibit large magnetocrystalline anisotropy, not observed in bulk. The spin can also be large or quenched by electronic effects such as the Kondo effect. In addition, coupling between spins can be via direct overlap, RKKY or superexchange. Secondarily, these systems are compelling because of their parallels with other nano-scale systems – quantum dots, magnetic multilayers and magnetic impurities in thin films, to name just a few. Finally, there are the possible applications to nano-scale magnetic bits and future magnetic devices. A large net spin and magnetic anisotropy are required for atomic-scale magnetic structures to be used as practical nano-scale magnetic bits. One possible way to obtain a large effective magnetic moment is through a ferromagnetic coupling between transition metal atoms. However, ferromagnetic coupling is rare in transition metal complexes,[2] that is, when the transition metal atom is bonded to a nonmetallic atom. We describe below our studies of such a system.

In a Scanning Tunneling Microscope (STM) measurement[3] of a Ti atom placed on a Cu2N/Cu(100) surface, it was found that the Ti exhibits very different magnetic properties than it does in gas phase. In the following work, we are able to verify these experimental findings and also explore additional properties of interest. We use density functional theory (DFT) to study the atomic spin of a single Ti atom, and the exchange coupling of a dimer of Ti atoms, placed on a single layer of Cu2N on a Cu(100) surface. The Cu2N layer is used as an insulating layer to isolate the spin of a magnetic adatom from the metal electrons of the Cu(100) surface[1,4]. Hereafter, the Cu2N/Cu(100) surface will be referred to as the CuN surface. We first calculate the adsorption energies and spin of Ti as a function of its coverage when it is deposited on top of Cu, on top of N and at hollow sites in the CuN surface. We study exchange coupling between Ti atoms in two different environments: (i) a square lattice of Ti on the CuN surface and (ii) a dimer of Ti atoms deposited on the CuN surface.

II. DFT CALCULATIONS

We use spin-polarized DFT, as implemented in Quantum-ESPRESSO[5], within a pseudopotential formalism using a plane wave basis with a cut-off of 30 Ry. A higher cut-off of 240 Ry was used for the augmentation charges introduced by the ultrasoft pseudopotential[6]. We use the generalized gradient approximation (GGA) for the exchange correlation interaction with the functional proposed by Perdew, Burke and Ernzerhof.[7] An on-site Coulomb interaction (U) for d-states of Ti was employed, with U taken to be 0, 3, 4.7, and 6 eV. The value of 4.7 is obtained using a constraint-GGA method[8,9]. To improve the convergence, a Gaussian smearing of width 0.01 Ry was adopted. Brillouin zone integrations for the (1×1) surface cell of Cu(100) were carried out using a $(16 \times 16 \times 1)$ mesh of k-points.

We obtained the bulk lattice parameter for Cu as 3.67 Å, which compares well with the experimental value of 3.61 Å[10]. To simulate the CuN surface, we use a symmetric slab of three to five atomic layers of Cu, with a layer of CuN above and below. Periodic images of the slab were separated by a vacuum of 15 Å along the z [100] direction.

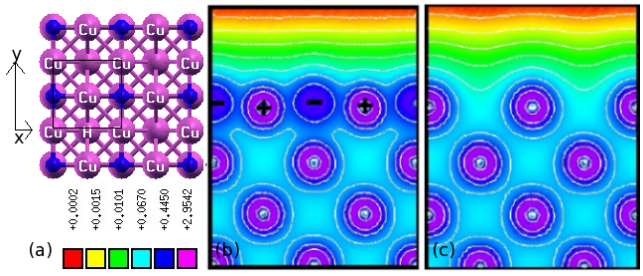

FIG. 1: (a) Top view of the CuN on Cu(100) surface; small and big spheres represent N and Cu atoms respectively. Big spheres with symbol "Cu" are the top layer Cu atoms and those without the symbol are the second layer. The black square indicates the c(1 × 1) unit cell of the CuN surface. Along the x-axis, surface Cu atoms are separated by a hollow site (it is marked by 'H') and along the y-axis, they are separated by a N atom. Side views of charge density produced by a cut along the (b) N-axis and (c) hollow-axis.

III. CUN SURFACE

The top view of the CuN surface is shown in Fig. 1a. The unit cell of the CuN surface (shown by the black square) consists of two Cu atoms and one N atom. We find that the N atoms are 0.18 Å above the top Cu atoms in a fully relaxed structure. The distance between the first and second layers of Cu is 1.97 Å which compares well with the all-electron result of 1.91 Å[11]. We find that each Cu atom in the surface unit cell loses 0.7 electrons to the N (presumably due to the electronegative nature of N). Thus, Cu and N atoms form a square network of dipoles on the surface, rendering a (nominally) insulating character to the surface. As shown in Fig.1a, along the x-axis, two surface Cu atoms are separated by a hollow site and along the y-axis, they are separated by a N-atom. These directions will be referred as hollow-axis and N-axis, respectively. The charge density of the CuN surface along the N- and hollow-axis is shown in Fig.1(b) and (c) respectively. Notice that along the N-axis, charge gets accumulated in the top layer. Similar charge distribution was observed from an all-electron calculation for the same system[4].

IV. SPIN OF TI ON CUN SURFACE

To calculate the spin of Ti on the CuN surface, we first determine the most stable binding site for Ti on the surface. In Fig.2, we plot the adsorption energy of Ti at various sites on the CuN surface as a function of Ti coverage. It is computed as $AE(Ti) = E(Ti/CuN) - E(CuN) - E(Ti_{gas})$; where first, second and third terms are the total energies of Ti adsorbed CuN surface, bare CuN surface, and single Ti atom in gas phase, respectively. Energy of the single Ti atom is calculated using a cubic unit cell of size 19 Å for U equal to 0 and 4.7 eV. Black and red symbols represent the adsorption energies for U=0 and U=4.7 eV, respectively. Notice that the adsorption energy decreases as U increases and, for a given value of U, Ti has the highest binding on top of Cu atoms compared with on top of N or at hollow sites, in agreement with STM experiments[3]. The total energy difference for the single Ti atom between U=0 and U=4.7 eV calculations is found to be 0.26 eV; the energy at U=4.7 eV is greater than the energy at U=0 eV. Thus, the difference in adsorption energy for the two values of U is not entirely due to the energy difference for the single Ti atom. When Ti is adsorbed at a hollow site, we find that Ti tends to go deep in the surface (for U=0), thereby distorting the surface significantly. However, as we increase U to 2.5 eV and 4.7 eV, the surface is not much distorted but the adsorption energy decreases.

Next, we calculate the spin of Ti in (1 × 1), (2 × 2), and (2 × 3) unit cells, i.e., at coverages of 1, 1/4, and 1/6 ML respectively. These calculations are done for U=0 and U=4.7 eV and the data is plotted in Fig. 2. Interestingly, as the coverage of Ti decreases, the spin of Ti nears the experimentally observed value of S=1/2 for U=0. Presumably, there are lower coverages of Ti in experiments as the scanning tunneling spectroscopy measurements were conducted on a single Ti atom. However, for U=4.7 eV, the spin of Ti starts at S=0.75 for high coverages and saturates at S=1 for low coverages. Notice that the spin of Ti on top of a N atom or at a hollow site is close to 1 even at U=0. At one monolayer coverage of Ti, the (1 × 1) surface unit cell consists of one N atom, one Ti atom and two Cu atoms, as shown in Fig.2. A constrained-GGA[8] calculation[9] yields U = 4.7 eV for Ti in this configuration. In order to understand the effect of U on the spin of Ti, we do calculations for a range of values of U for the (1 × 1) unit cell. The results for distances between Ti and its nearest neighbor atoms in the surface, angle subtended by Ti-N-Ti, and the spin of Ti are shown in Table I. We find that Ti-N and Ti-Cu distances increase as U increases, with the net effect of a rising Ti and decreasing (becoming sharper) Ti-N-Ti angle. Most importantly, as U increases, the spin of Ti approaches that of the gas phase value of 1. Comparable to the (1 × 1) unit cell, the distance of Ti from the Cu below in (2 × 2) is 2.58 Å. There is also a similar trend of Ti rising higher above the surface than N, by an amount increasing with increasing U. Most importantly, it was found that in all three cases of larger unit cells, the spin of Ti is 1 for non-zero values of U.

Additional complexity was encountered, as it was found that the initial magnetization of Ti affects the final calculated ground state, indicating a complex energy minimization landscape. Hence we tried several initial magnetizations and take the final state that corresponds to the lowest energy. For U=4.7, we show the data corresponding to two such optimized structures (S-I and S-II) obtained by varying the initial magnetization (see Table I). The optimized structure corresponding to S-I is the lowest energy structure (S-I is lower in energy than S-II

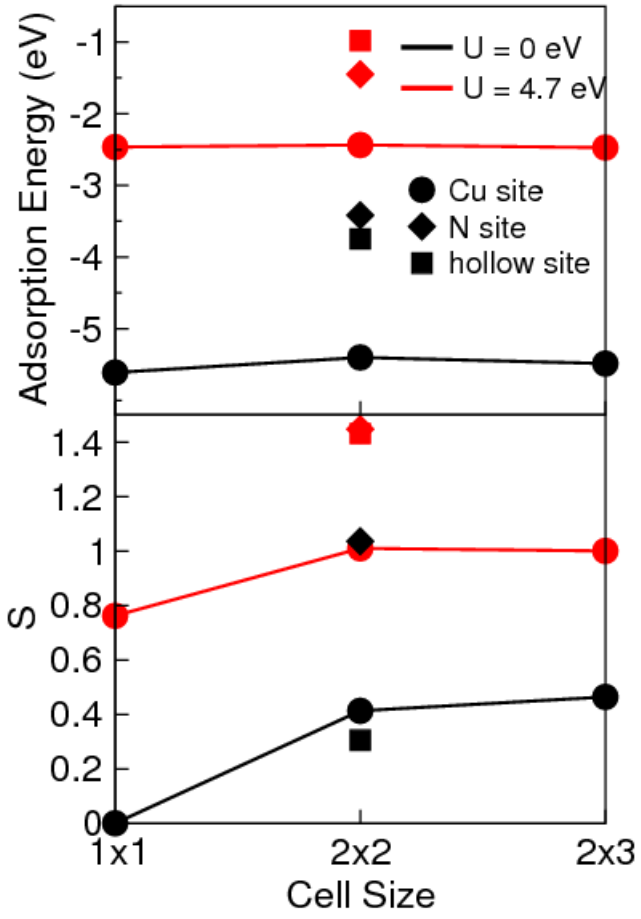

FIG. 2: Adsorption energy and S of Ti as a function of cell size for U=0 (black) and U=4.7 eV (red). As the cell size increases, coverage of Ti decreases. Filled circles, diamonds, and squares represent the adsorption energy of Ti on top of a Cu atom, on top of a N atom, and at hollow sites, respectively.

by 0.3 eV), showing the spin of Ti to be 0.75, indicating possible mixed valent behavior for a monolayer of Ti.

V. EXCHANGE COUPLING

To calculate the exchange coupling, we assume a Heisenberg interaction ($H = J\mathbf{S_1}.\mathbf{S_2}$), and can relate the value of J to the energy difference between ferromagnetic and (Ising) antiferromagnetic configurations:

$$2S^2J = E_{\uparrow\uparrow} - E_{\uparrow\downarrow} \equiv \Delta E \qquad (1)$$

Here, S is the magnitude of spin, and J is the exchange coupling. $E_{\uparrow\uparrow}$ and $E_{\uparrow\downarrow}$ are the total energies calculated from DFT when the spins on the magnetic atoms point along the same direction and in opposite directions respectively. Note that Eq. 1 holds for all values of quantum spin. The relationship with J is valid for each S^z always at full maximal or minimal value (Ising antiferromagnet; collinear spins); for the energy difference with

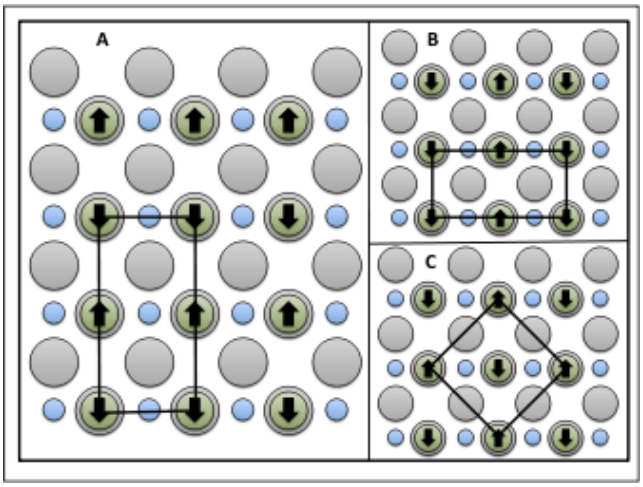

FIG. 3: Schematic diagrams showing spin configurations in Ti lattices. In configuration (a), spins are aligned along the N-axis and antialigned along the hollow-axis; in (b) spins are antialigned along the N-axis and aligned along the hollow-axis. Configuration (c) is a checkerboard configuration with spins antialigned along both the N- and hollow-axis.

a full quantum antiferromagnetic state, the term $2S^2J$ would become $(2S+1)SJ$. In this paper, we will mainly concentrate on the energy difference between ferromagnetic (aligned) and antiferromagnetic (antialigned) configurations, rather than on the value of J. We calculate the exchange coupling for Ti lattices (1ML coverage of Ti) and for two Ti atoms placed on the CuN surface in a large unit cell.

A. Lattice of Ti atoms on CuN surface

At one monolayer coverage of Ti on CuN surface, Ti forms a square "lattice" on the surface. In this case, the energy of the ferromagnetic configuration (E_{FM}) is the total energy of the (1×1) unit cell since it contains only one Ti atom. However, to obtain $E_{\uparrow\downarrow}$, we design three different configurations with (1×2), (2×1), and $(\sqrt{2}\times\sqrt{2})$ unit cells as shown in Fig. 3(a), (b), and (c) respectively. Arrow signs in the figure indicate relative direction of spins on Ti atoms. Total energies of the three configurations will be referred to as E_H, E_N, and E_C respectively. Notice that the unit cell size in all three configurations is twice that of the ferromagnetic configuration. Subtracting the total energies of configurations (a), (b), and (c) from two times the energy of the ferromagnetic configuration $(2 \times E_{FM})$ will give the exchange coupling of Ti atoms along the hollow-axis, along the N-axis, and in the checkerboard configuration, respectively; assuming that there are only nearest neighbor interactions.

Our results for exchange coupling are summarized in Table II. For the lowest energy structure S-I, we find that the exchange coupling along the N-axis is unexpectedly ferromagnetic, i.e., the total energy E_{FM} is lower

System	Cell	U	d_{Ti-N}	d_{Ti-Cu}	$A_{Ti-N-Ti}$	S
Single Ti Atom	1×1	0.0	1.91	2.49	148.6	0.0
		3.0	1.95	2.54	141.6	0.6
		4.7 (S-I)	**1.99**	**2.56**	**135.6**	**0.75**
		4.7 (S-II)	2.27	2.68	108.4	1.0
		6.0	2.33	2.72	104.2	1.0
	2×2	4.7	2.07	2.58	-	1.0
	2×3	3.0	1.98	2.52	-	1.0
	3×3	6.0	2.13	2.66	-	1.0
Ti Dimer	N-axis	4.7	2.04	2.65	142.9	1.0
	H-axis	4.7	2.09	2.56	-	1.0

TABLE I: The Ti-N bond length (d_{Ti-N}), the Ti-Cu bond length (d_{Ti-Cu}), the Ti-N-Ti angle ($A_{Ti-N-Ti}$) and the spin S of the Ti atom on the CuN surface. The top panel shows these results as a function of Hubbard U (in eV) on Ti, for a (1×1) unit cell. The middle panel shows these results for a single Ti atom in (2×2), (2×3), and (3×3) unit cells. The bottom panel shows these results for a dimer of Ti adsorbed along the N- and hollow-axis, respectively. All the bond lengths are given in Angstroms.

than E_N by 16.1 meV. However, the exchange coupling across a hollow is antiferromagnetic, i.e., the total energy E_H is lower than E_{FM} by 106.8 meV. Thus, the antiferromagnetic coupling along the hollow-axis is much stronger than the ferromagnetic coupling along the N-axis. The checkerboard pattern (Ising antiferromagnet) is more favored over a pure ferromagnetic state with ΔE being 77.8 eV; however, it is less favorable than the hollow-axis antiferromagnetism, presumably due to the energy disadvantage of antiferromagnetic coupling along the N-axis. The overall order, from lowest to highest energy, is $E_H < E_C < E_{FM} < E_N$. Configuration Fig. 3a is the ground state and we term it a spin striped state. These ferromagnetic stripes should be observable in large enough lattices.

In order to understand how structure plays a role in the exchange coupling, we also calculate spin exchange for the structure S-II (Table II). We notice that the exchange coupling for the structure S-II is much lower than that of S-I. This could possibly be due to lower interaction of Ti with the surface (See Table-I, Ti-Cu and Ti-N distances are longer in S-II than those in S-I). Spin density plots for the two structures in the ferromagnetic state are shown in Fig.4. Notice that the spin density gets stretched out along the hollow-axis for S-I. Also, the N atoms get spin polarized for S-I more than for S-II. This shows that in S-I, there are stronger interactions. The net result is that this structure has the lowest total energy.

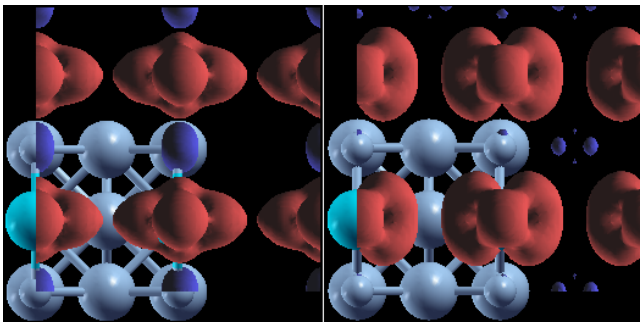

FIG. 4: Spin density plot for (1×1) unit cell for lower energy (a) and higher (b) configurations. Different colors (shadings in black and white version) correspond to opposite spins. The Nitrogen atoms appear as small spheres with opposite polarization between the Ti.

System	Structure	$E_{FM} - E_N$	$E_{FM} - E_H$
Lattice 1×1	S-I	-16.1	106.8
	S-II	6.2	13.9
Dimer 2×3	-	-16.5	143.9

TABLE II: The energy differences ΔE (in meV) along the N-axis ($E_{FM} - E_N$) and the hollow-axis ($E_{FM} - E_H$) for a lattice of Ti in a (1×1) unit cell, and a dimer of Ti in a (2×3) unit cell.

B. Dimer of Ti atoms on CuN surface

We have drawn conclusions so far about Ti-Ti coupling based on the calculations in lattices, where the situation is more complicated because one not only has the nearest neighbor (NN) interactions but also has next NN (NNN) interactions and so on. To simulate a Ti-Ti dimer on the surface we use a larger unit cell of (2×3) with two and three lattice units along the hollow- and N-axis respectively. Interestingly, we find ferromagnetic coupling along the N-axis and antiferromagnetic along the hollow-axis, the same ground states as for the case of (1×1) lattices. Along the N-axis, the energy difference (ΔE) is -16.5 meV compared to -16.1 meV for the (1×1) case. Along the hollow-axis the energy difference is 143.9 meV compared to 106.8 meV for the (1×1) case. Thus, a Ti lattice and a dimer show a similar trend and strength of coupling. It confirms our assumption of primarily nearest neighbor interactions in a Ti lattice on the CuN surface.

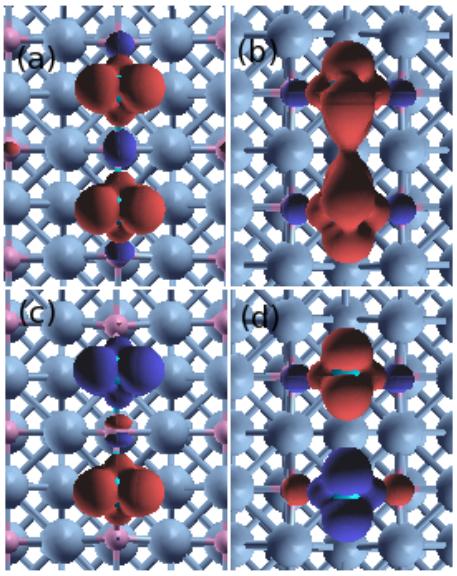

FIG. 5: Spin density ($\rho_\uparrow - \rho_\downarrow$) plot for ferromagnetic (top pannel: (a) and (b)) and antiferromagnetic (bottom pannel: (c) and (d)) configuration of a Ti dimer along the (a) N-axis and (b) hollow-axis. The most energetically favorable configurations are ferromagnetic across a N (top left) and antiferromagnetic across a void (bottom right).

To obtain exchange coupling, one would simply divide the energy differences given in Table II by 2S(S+1), where values of spin on Ti atoms are given in Fig. 2 and in Table I. Notice that the distance between Ti and the Cu atom below it is 2.56 Å for both the (1×1) case, and the (2×3) case for coupling along the hollow-axis. However, when the dimer is placed along the N-axis the distance between Ti and the Cu below it increases slightly to 2.65 Å. The Ti-N-Ti angle is 135.6 degrees for the (1×1) case which is close to 142.9 degrees for the (2×3) case.

In Fig. 5, we plot the spin density for the Ti dimer along the N-axis (Fig.5a) and the hollow-axis (Fig.5b). A significant amount of induced spin-polarization around the N atom can be seen from the figure. Ferromagnetic coupling between Ti atoms along the N-axis is established by having an opposite spin N atom both between the Ti atoms and at opposite ends. For anti-aligned spin configuration along the N-axis, the N atom becomes a single-atom antiferromagnet with a net spin of zero. Along the hollow-axis, when spin on both the Ti atoms is aligned, a dramatic anisotropy in the spin polarization of the Ti develops, with a direct overlap established over the hollow site (Fig.5b). The stretching of the Ti bonds in this case case is striking, and suggestive that higher symmetry considerations may be coming into play. However, when spins are antialigned, no such elongation of spin polarization occurs. In both the cases, N atoms on the sides of the two Ti atoms develop a spin polarization opposite to that of the Ti.

The primary sources of exchange coupling between the Ti atoms are superexchange[12], RKKY[13], and direct overlap/direct exchange[10]. The coupling between the adatoms can be direct, if the wave functions should overlap, or RKKY, if the influence of the Cu in the layers below is strong enough. Along the N-axis, the center N atom becomes a natural source for a superexchange coupling between Ti atoms, ruling out RKKY which would need to take an indirect route under the N atom, a much longer route than directly across the N for superexchange. Along the hollow-axis, however, there is no convenient single atom to hop across for superexchange, rather the sea of conduction electrons from the underlying and intervening Cu. (Unless one is to consider superexchange via the second-layer Cu, an unlikely candidate.) In this case RKKY and direct overlap become more likely. Indeed for an aligned spin configuration, we observe a direct overlap forming, as discussed above. However, the lowest energy state for coupling along the hollow-axis is antiferromagnetic, and we conclude that in this case it is likely due to RKKY coupling. This could be tested experimentally by varying the Ti-Ti distance and measuring the exchange coupling; however, only certain discrete lattice positions would be possible.

VI. CONCLUSIONS

In agreement with experiments[4], we find that Ti has the highest adsorption energy when deposited on top of a Cu atom. We find that the spin of Ti atoms varies with the coverage. For low coverages of Ti, the spin of Ti is 0.5, which is an experimentally observed value[4]. However, the spin of Ti becomes 1 as the value of U is increased even at low coverages.

We find a ferromagnetic coupling along the N-axis and antiferromagnetic along the hollow-axis, for both the lattice and dimer of Ti on the CuN surface. Ti lattice and dimer have a similar trend as well as strength of coupling. This indicates that interactions between Ti atoms in the lattice configuration are local; and a marked spin striped phase is found as the ground state of the lattice. We find a ferromagnetic coupling along the N-axis due to superexchange, with secondary contributions from direct exchange. We also postulate that the antiferromagnetic coupling along the hollow-axis is primarily due to RKKY interactions, with a smaller direct exchange component.

[1] C. F. Hirjibehedin, C. P. Lutz, and A. J. Heinrich, Science **312**, 1021 (2006).
[2] O. Kahn, *Molecular Magnetism* (VCH Publishers, 1993).
[3] A. F. Otte, M. Ternes, K. von Bergmann, S. Loth, H. Brune, C. P. Lutz, C. F. Hirjibehedin, and A. J. Heinrich, Nature Physics **4**, 847 (2008).

[4] C. F. Hirjibehedin, C.-Y. Lin, A. F. Otte, M. Ternes, C. P. Lutz, B. A. Jones, and A. J. Heinrich, Science **317**, 1199 (2007).
[5] S. Baroni, A. D. Corso, S. de Gironcoli, and P. Giannozzi (http://www.Quantum-Espresso.org, 2003).
[6] D. Vanderbilt, Phys. Rev. B **41**, 7892 (1990).
[7] J. P. Perdew, K. Burke, and M. Ernzerhof, Phys. Rev. Lett. **77**, 3865 (1996).
[8] G.K.H.Madsen and P.Novák, Europhys. Lett. **69**, 777 (2005).
[9] t. b. p. C.-Y. Lin.
[10] N. W. Ashcroft and N. D. Mermin, *Solid State Physics* (Saunders Company, 1976).
[11] M. A. Barral, R. Weht, G. Lozano, and A. Llois, Physica B **398**, 369 (2007).
[12] A. Bencini and D. Gatteschi, *EPR exchange coupled systems* (Springer Verlag, 1990).
[13] M. Ruderman and C. Kittel, Phys. Rev. **96**, 99 (1954); T. Kasuya, Prog. Theor. Phys. **16**, 45 (1956); K. Yosida, Phys. Rev. **106**, 893 (1957).